Evolution of enduring contacts and stress relaxation in a dense granular medium

Duan Z. Zhang

Theoretical Division, Fluid Dynamics Group, T-3, B216, Los Alamos National Laboratory, Los Alamos, New Mexico 87545, USA

(Received 26 July 2004; revised manuscript received 3 January 2005; published 15 April 2005)

Particle contacts in a granular material are formed at different times and have different contact ages, the differences between current time and the times when the contacts were formed. The probability distribution of the contact ages is one of the important statistical properties of particle interactions. The rate of the probability relaxation is proved to be closely related to the stress evolution in the dense granular system. While all particle contacts contribute to the stress, the major contribution is from the contacts with long contact ages compared to the binary collision time of the particles in a dense and slow granular flow, in which particle inertia can be neglected. There is a spectrum of relaxation times in the probability distribution of contact ages. These relaxation times result in different time scales of stress relaxation. As an example, the relations among stress, strain, and the strain rate are studied for a dense granular material undergoing an oscillatory simple shear. The interaction of the time scales determines the fluidlike or solidlike behavior of the material.

DOI: 10.1103/PhysRevE.71.041303 PACS number(s): 45.70.−n, 45.05.+x, 47.50.+d, 45.70.Cc

I. INTRODUCTION

Kinetic theories have been used successfully for the study of granular flows in which particle interactions are primarily instantaneous binary collisions [1–4]. The assumption of instantaneous binary collisions hampers the application of the theory to many practical problems [5]. Attempts have been made to amend this deficiency in the kinetic theory [6]. In that work the binary contact time is added to the mean free flight time to reduce the particle collision frequency. Only binary collisions are considered. In many practical granular flows, such as granular flow down an incline [7], multiparticle interactions are common and contact times are much longer than the binary collision time because of multiparticle interactions. Particle interactions dissipate a large amount of energy and prevent many practical granular systems from becoming rapid granular flows. Recent work of Campbell [5] and Louge [7] indicates that a dense granular flow model has to account for enduring multiparticle contacts. The present paper studies the statistical behavior of enduring multiparticle or cluster interactions and their effects on the evolution of the granular stress in dense (approaching to the close-packed volume fraction) granular systems consisting of deformable particles.

Interactions among particles result in a contact stress in a granular material. This stress is the major stress in a dense granular material and the stress resulting from fluctuations in particle velocities is negligible because the confinement provided by neighboring particles significantly reduces velocity fluctuations. The contact stress can be calculated from the average interaction force between a pair of contacting particles and the pair distribution function [8,9]. The use of pair distribution function does not imply binary interactions. The evolution of the pair distribution depends not only on the interaction between the pair of particles but also depends on their interactions with other particles surrounding the pair. Microstructures, including particle clusters and force chains, affect the evolution of the pair distribution function. However, the pair distribution function itself only explicitly carries information about spatial correlations and does not explicitly carry information about the evolution of the contacting pair. In the present work, a contact probability distribution is introduced to include both the spatial and temporal correlations of particle contacts. Particle contact age, defined as the difference between the current time and the time when the contact was formed, is explicitly included in the contact probability distribution. Without multiparticle interactions, the age of a contact cannot exceed the binary collision time. For a dense granular flow the durations of contacts can be much longer than the binary collision time. The significant disparity between the binary collision time and the particle contact age carries information about multiparticle interactions. In the present paper we show the important relationship between the relaxation of the contact stress and the probability distribution of contact ages.

Although finding closures is one of the main objectives of granular flow research, the primary intention of the present work is focused on interactions of time scales in dense granular flows and the development of proper statistical tools to describe these interactions. To find closures for dense granular flow, not only the interactions of time scales, but also the interactions of length scales and the interactions among the time and length scales are important. There are many other works devoted to the study of length scales in granular flows, including particle clusters, force chains and crystallizations [11]. Little attention has been paid to interactions of time scales of dense granular flows.

In Sec. II, we study the probabilities that are important to the time scales of particle interactions. The relaxation time of particle contacts is introduced. Although these equations are unclosed, they relate various quantities important to particle interactions. These relations represent many interesting physics of various particle interactions, ranging from binary collisions to cluster interactions.

The quantities introduced in Sec. II are studied numerically in Sec. III. In the case of steady simple shear flow, the evolution equation for the probability distribution of contact ages introduced in Sec. II can be solved for long-term contacts. The solution is in good agreement with numerical results. The equations obtained in Sec. II are used in Sec. IV to derive an evolution equation for the contact stress. The relaxation times of the age probability distribution are shown to be the stress relaxation times. Many observed properties of the stress can be explained by the behavior of the probability distribution of ages, which is a result of multiparticle interactions at different time scales.

Although the statistical description of particle interactions introduced in the present paper is applicable to polydisperse systems, to emphasize the physics in the description and to avoid unnecessary mathematical complications, we restrict ourselves to a granular system consisting of identical deformable spherical particles.

II. CONTACT PROBABILITY AND ITS RELAXATION TIME

To study enduring contacts in a dense granular flow, we need to know the ages of contacts in the granular system. The age in a contact is defined as the difference between the current time and the time when the contact was formed. Contact formations are random events in a granular system; therefore, the contact age is a random variable. We now introduce a contact probability density $P_s(\mathbf{x},\theta,\phi,a,t)$ to describe its distribution. This probability density is a function of the position $\mathbf{x}$ in space, the orientation represented by the polar angle θ and the azimuthal angle ϕ in the spherical coordinate system centered at $\mathbf{x}$, the contact age a, and the time t. This probability is defined in such a way that, at time t, $P_s(\mathbf{x},\theta,\phi,a,t)dxdydz \sin\theta d\theta d\phi da$ is the probable number of contacts in the volume $dxdydz$ about the spatial point $\mathbf{x}$, with orientations of the contacts in the solid angle $d\omega = \sin\theta d\theta d\phi$ about the direction represented by the polar angle θ and the azimuthal angle ϕ and with contact ages between a and $a+da$. This probability density is normalized to the number of contacts in the system instead of one. The integration of this probability density over all possible angles and ages yields the contact density $n_c(\mathbf{x},t)$, the number of contacts per unit volume:

$$n_c(\mathbf{x},t) = \int_0^\infty \oint P_s(\mathbf{x},\theta,\phi,a,t)d\omega da. \tag{1}$$

The definition of the probability density P_s introduces a six-dimensional parameter space. There are three dimensions associated with the center of one of the particles in the pair, two dimensions associated with the orientation of the contact, and one dimension associated with the contact age. We note that along the dimension of age we always have $da/dt=1$. Following the usual procedures for the derivation of the continuity equation in fluid dynamics or the similar procedures [10] for the derivation of the Liouville equation in a parameter space, we can derive the evolution equation for the probability density P_s as follows. For a small control volume $dV_6 = dxdydz \sin\theta d\theta d\phi da$ in the six-dimensional parameter space during a short time duration dt, the increase $(\partial P_s/\partial t)dV_6 dt$ in the probable number of contacts in the small control volume equals the difference between the probable number of contacts moving into the control volume through the enclosing surfaces, which can be calculated as $-\boldsymbol{\nabla}_6\cdot(\mathbf{v}_6 P_s)dV_6 dt$, and $P_s/\tau dV dt$, the probable number of contacts that break during the time duration dt,

$$\frac{\partial P_s}{\partial t}dV_6 dt = -\boldsymbol{\nabla}_6\cdot(\mathbf{v}_6 P_s)dV_6 dt - \frac{P_s(\mathbf{x},\theta,\phi,a,t)}{\tau(\mathbf{x},\theta,\phi,a,t)}dV_6 dt. \tag{2}$$

There is no term representing contact generation in this equation because no contact can be generated with age $a>0$. In other words, the contribution of contact generation is represented by the probability $P_s(\mathbf{x},\theta,\phi,a,t)$ with age $a=0$. The divergence of the contact flux in the six-dimensional space can be calculated as

$$\boldsymbol{\nabla}_6\cdot(\mathbf{v}_6 P_s) = \frac{\partial P_s}{\partial a} + \boldsymbol{\nabla}_{\mathbf{x}}\cdot(\overline{\mathbf{w}}P_s) + \frac{1}{\overline{r}\sin\theta}\left[\frac{\partial(\overline{v_\theta}\sin\theta P_s)}{\partial\theta} + \frac{\partial(\overline{v_\phi}P_s)}{\partial\phi}\right], \tag{3}$$

where $\overline{\mathbf{w}}$ is the averaged velocity of the particle located at $\mathbf{x}$, $\overline{r}$ is the averaged distance between the contacting particles, and $\overline{v_\theta}$ and $\overline{v_\phi}$ are the polar and azimuthal components of the averaged relative velocity between the contacting particles in the spherical coordinate system with the origin at $\mathbf{x}$. The overbars in this equation denote the average under the condition that at time t there is a particle centered at $\mathbf{x}$ contacting another particle in the direction (θ,ϕ) with contact age a. In Eq. (2), $1/\tau$ is the contact breakage rate per contact. For convenience, we use the relative angular velocities $\overline{\dot{\theta}}$ and $\overline{\dot{\phi}}$ instead of the relative velocity components $\overline{v_\theta}$ and $\overline{v_\phi}$ in the rest of the paper. These velocities are related by $\overline{v_\theta}=\overline{r\dot{\theta}}$ and $\overline{v_\phi}=\overline{r}\sin\theta\dot{\phi}$.

Using the relative angular velocities, one can rewrite the evolution equation 2 for P_s as

$$\frac{\partial P_s}{\partial t} + \frac{\partial P_s}{\partial a} + \boldsymbol{\nabla}_{\mathbf{x}}\cdot(\overline{\mathbf{w}}P_s) + \frac{1}{\sin\theta}\frac{\partial(\overline{\dot{\theta}}\sin\theta P_s)}{\partial\theta} + \frac{\partial(\overline{\dot{\phi}}P_s)}{\partial\phi} = -\frac{P_s(\mathbf{x},\theta,\phi,a,t)}{\tau(\mathbf{x},\theta,\phi,a,t)}. \tag{4}$$

Before this equation can be used to solve for the contact probability density P_s, closures for these conditionally averaged velocities and a closure for the relaxation time τ need to be found. Finding general closure relations for these quantities is not the purpose of the current paper. Instead, in the current work we study properties of the contact probability density P_s for the case of simple shear flow by directly calculating the probability from the results of numerical simulations. Despite the obvious importance of the relative angular velocities $\overline{\dot{\theta}}$ and $\overline{\dot{\phi}}$ to the understanding of particle interactions, the present work focuses on the understanding of the effects of the relaxation time τ in the case of simple shear flows and leaves the study of the influence of averaged relative angular velocities $\overline{\dot{\theta}}$ and $\overline{\dot{\phi}}$ to future work. Priority is given to the study of the relaxation time because this relaxation time corresponds to the stress relaxation time as shown in Sec. IV, and the effects of pertinent time scales in granular flow have rarely been studied.

The probability density P_s is a function of seven variables. To facilitate the study of its properties we decompose it into conditional probabilities as follows:

$$P_s(\mathbf{x},\theta,\phi,a,t) = n_c(\mathbf{x},t)P_g(a|\mathbf{x},t)P_d(\theta,\phi|\mathbf{x},t,a), \qquad (5)$$

where n_c is the contact density as defined in Eq. (1), P_g is the probability distribution of contact ages, regardless of contact angular orientations but conditional on the event of one of the contacting particles being located at the position $\mathbf{x}$ at time t, and P_d is the probability distribution of contact directions conditional on one of the contacting particles being located at position $\mathbf{x}$ at time t and with the contact age a. In these definitions, the probabilities P_g and P_d normalize to 1.

In the next section we calculated these conditional probabilities in numerical simulations of statistically steady simple shear flows in a statistically homogeneous medium. In this case the contact density n_c is a constant, and all of the probabilities are independent of position $\mathbf{x}$ and time t.

III. CONTACT AGE PROBABILITY UNDER SIMPLE SHEAR FLOW

Simple shear flows have been studied extensively; many macroscopic properties, such as stresses, are well known. In this section, we use simple shear flows as examples to study the probabilities introduced in the last section. Numerical results in this section are obtained from three-dimensional numerical simulations of an assembly of monodisperse spheres using a scheme described in earlier papers [8,9].

For steady simple shear flows in a statistically uniform medium, n_c, P_g, and P_d are independent of $\mathbf{x}$ and t. By integrating θ and ϕ over an entire sphere, the probability evolution equation (4) becomes

$$\frac{\partial P_g}{\partial a} = -\frac{P_g}{\tau_g(a)}, \qquad (6)$$

where

$$\frac{1}{\tau_g(a)} = \oint \frac{P_d(\theta,\phi|a)d\omega}{\tau(\theta,\phi,a)} \qquad (7)$$

is the contact breakage rate averaged over all directions.

Randomness of particle interactions results in the loss of memory and therefore the rate of contact breaking, or τ_g, is independent of the age a for long contacts [9]. Under this condition, Eq. (6) can be solved to find that the contact age distribution P_g approaches an exponential distribution for large contact ages. The reasoning used to reach this conclusion is independent of the force models. To demonstrate this conclusion we simulate a simple shear flow using the following force model. The normal force F_n is modeled as a parallel connection of a spring and a dashpot:

$$F_n = -K_n\left(\frac{\Delta_n}{R}\right)^p + R_e v_r, \qquad (8)$$

where K_n is a constant related to the stiffness of the particles, R is the particle radius, $\Delta_n = 2R - r$ is the compressive defor-

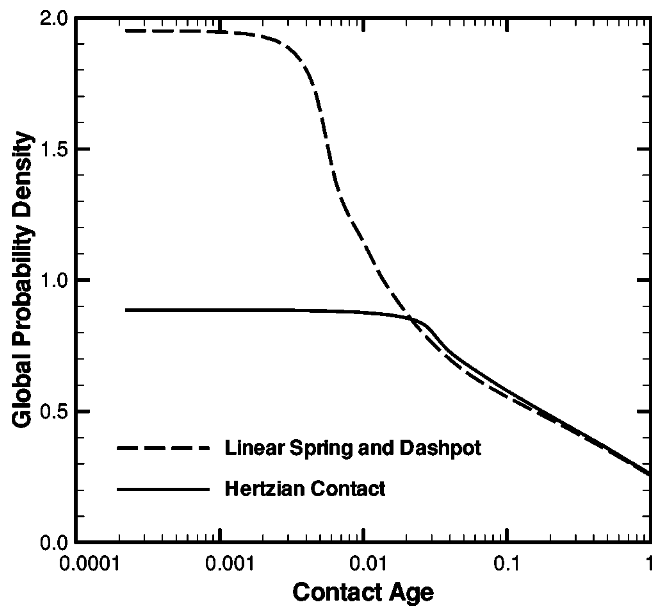

FIG. 1. The probability distribution for short contact ages for two different force models. In this example, the constant K_n in Eq. (8) is 2.0×10^5 and resistance of the dashpot is 20.04. For the case of the linear spring and dashpot normal force model the corresponding normal restitution coefficient e_n is 0.902 in a binary collision.

mation of the contacting particle pair, R_e is the resistance of the dashpot, and v_r is the relative normal velocity. The power p can be set to be 1.0 to obtain the linear spring and dashpot force model and set to $3/2$ to obtain the Hertzian force model. Tangential forces are calculated according to the tangential deformation built up during the particle contact [9]. Tangential slip is allowed when the tangential force exceeds μF_n, where μ, the friction coefficient, is set to 0.3 in the calculations.

In the numerical calculation, the mass is nondimensionalized by the mass of the particles and the length is nondimensionalized by the particle radius. The mass and particle radius are set to unity. The time in the calculation is nondimensionalized by considering the oscillator consisting of two mass points with mass m at both ends of a linear spring with constant K_n/R, which has a period $\pi\sqrt{2mR/K_n}$. A time unit in the calculation is set to be 100 periods.

The probability distributions for a simple shear flow with the nondimensional shear rate 0.1 and the particle volume fraction 0.6 are calculated using $p=1$ and $p=3/2$. For small contact ages, the difference is evident as shown in Fig. 1. The plateau of the age distribution is associated with the binary collision time. When the normal force is modeled as a parallel connection of a linear spring and a dashpot, the binary collision time is independent of relative velocity of the interacting pair and is calculated to be 5.0×10^{-3}, about the age that the plateau ends for the case plotted in the figure. The binary collision time for the Hertzian force model depends on the relative velocity of the colliding pair. If we estimate the averaged relative velocity as the product of the shear rate and the averaged distance between the particles, the binary collision time is about 2.3×10^{-2}, which is in agreement with the age that the plateau ends for the case

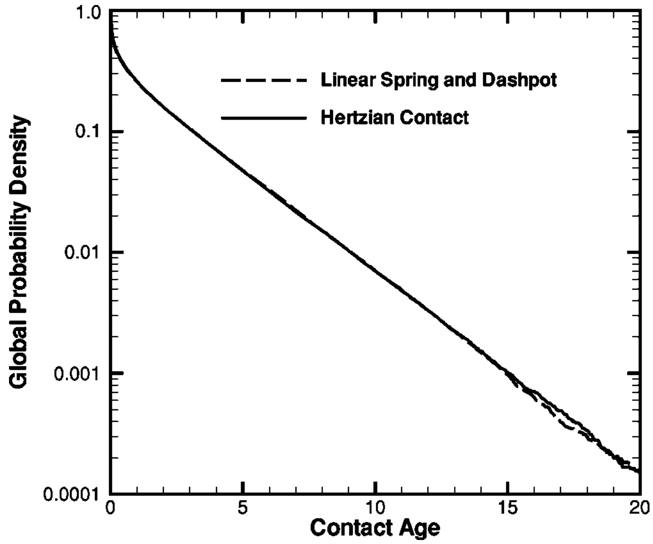

FIG. 2. The probability distribution for long contact ages. For long contact ages, the probability distributions for two different normal force models with the same friction coefficient are almost the same except for contact ages greater than 15. At these ages, the number of samples becomes small and large statistical errors appear.

plotted in the figure. These numerical examples show that the rate of probability relaxation depends on the contact age and the model of the particle interaction forces for contact ages that are not significantly larger than the binary collision time.

The results for long contact ages are plotted in Fig. 2. As predicted, for long ages, in both cases the probability distributions of ages obey the exponential distribution indicating that the probability relaxation rate $1/\tau_g$ is independent of age. It is reported [9] that the probability relaxation rate is a function of the friction coefficient between particles. The two cases plotted in Fig. 2 are calculated with the same friction coefficient. The little difference between the two cases suggests that the probability distribution is insensitive to normal force models for long-term contacts. The small difference seen for ages larger than 15 is due to the diminishing statistical samples at these contact ages.

In a dense granular system, particles often form clusters and there are two different types of contacts. In the first type, particles do not belong to any cluster and bounce back and forth among particles. The time scale for this type of contact to break is the binary collision time as shown in Fig. 1. In the second type of contact, particles belong to clusters that are tightly squeezed. The force and thus the stress resulting from this type of contact are large compared to that in first type of contact. To break such contacts, the neighboring particles need to move in a correlated fashion to make space for the particles. Therefore a contact of the second type is less likely to break and the contact ages of this type of contact are much larger than the binary collision time. However, breaking such a contact causes significant relaxation of the stress since the particle interaction forces in the second type of contact are much larger than the forces in the first type of contact. The time scale to make spaces available for contacts of the second type to break is determined by the motion of the clusters in the granular material. For a slow granular flow in which particle inertia is not important, the time scale of breaking contacts of the second type is determined by $1/\gamma$ since this is the only time scale available [9]. Therefore the breakage rate of the second type of contact is controlled by the motion of the clusters, and the relaxation time is of the order of the macroscopic strain rate as shown in Fig. 2.

The direction in which one can find the most contacts with a specified age is described by the probability distribution P_d. Since finding a contact with specific age is a zero possibility event, instead of evaluating P_d directly from the results of numerical simulation, we study its age average $[P_d]$, defined as

$$[P_d] = \frac{\int_b^c P_s(\mathbf{x},\theta,\phi,a,t)da}{n_c(\mathbf{x},t)\int_b^c P_g(a|\mathbf{x},t)da} = \frac{\int_b^c P_d(\theta,\phi|\mathbf{x},a,t)P_g(a|\mathbf{x},t)da}{\int_b^c P_g(a|\mathbf{x},t)da}, \tag{9}$$

for contacts with ages between b and c. The second equality is obtained by using Eq. (5). In the steady simple shear flow, the probabilities in Eq. (9) are independent of time. The averaged probability $[P_d]$ can be calculated by counting the number of contacts belonging to the age group (b,c) on the particle surface. A spherical coordinate is imposed on the particle surface with $\theta=0$ in the upward (z) direction and $\phi=0$ in the x direction, the direction of flow. The simple shear flow is simulated in a cubic box with periodic boundary conditions. The origin of a Cartesian coordinate is set at the center of the cubic box. The mean velocity of the particles is in the x direction and is set to γz. The particle surface is divided into 18×36 regions with 18 equal rows along the latitude and 36 equal columns along the longitude. After a steady state is reached, contacts are sorted according to region and age groups. For an age group (b,c), the value of $[P_d]$ at the center of a surface region is calculated as the number of contacts with ages between b and c in the surface region divided by total number of contacts within the age group on the entire spherical surface, divided by the solid angle of the region.

If the integrals in Eq. (9) are over the age interval $(0,\infty)$, the averaged $[P_d]$ is the probability distribution over the particle surface regardless of age. The result of this probability distribution is shown in Fig. 3 for the case of a linear spring $(p=1)$ and dashpot force model with the nondimensional shear rate 0.1 and particle volume fraction 0.6. The maximum of the probability density $[P_d]$ on the particle surface is not in the direction of principal compression, which is the direction $\theta=3\pi/4$, $\phi=0$ or $\theta=\pi/4$, $\phi=\pi$ in spherical coordinates. The maximum appears near the two stagnation points on the equator, which are in the directions of $\theta=\pi/2$, $\phi=0$ and $\theta=\pi/2$, $\phi=\pi$. This is because, in a simple

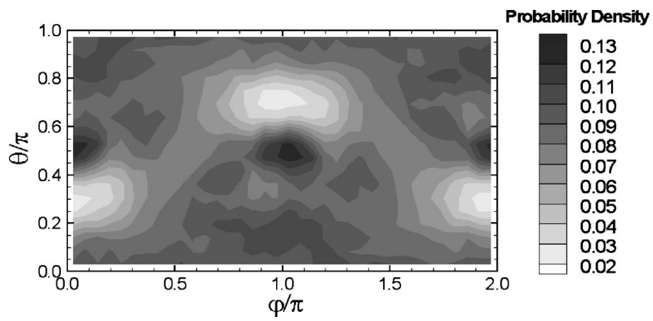

FIG. 3. Probability density of particle contacts on the particle surface regardless of age. Particle contacts are more likely to be in the dark regions than the light regions.

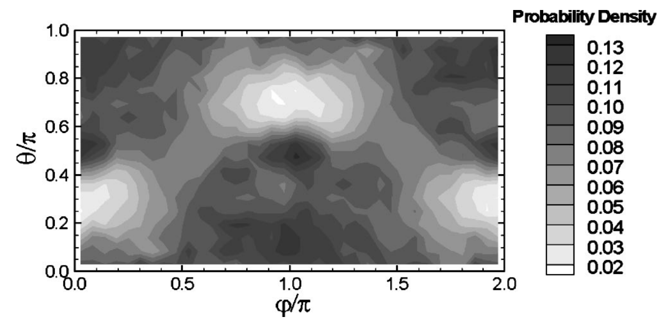

FIG. 5. Probability density of particle contacts on the particle surface for contact ages between 2 and 3 time units.

shear flow, there is a tendency for particles to form layers along the direction of shear so that particles can pass each other with the least resistance. A similar probability distribution of particle contact directions is observed in numerical simulations performed in a two-dimensional domain [11].

For age groups 0 to 0.01, 2 to 3, and 4 to ∞, results of the averaged probability $[P_d]$ are plotted in Figs. 4–6. The probability distribution $[P_d]$ plotted in Fig. 4 for short contact ages is quite different from the probability distributions plotted in Fig. 4 and 5, indicating that the probability distribution $P_d(\theta,\phi|\mathbf{x},a,t)$ is a strong function of age for ages comparable to the binary collision time. The local maxima appearing near $(\theta,\phi)=(0.1\pi,0)$ and $(0.9\pi,\pi)$ in Fig. 4 and near $(\theta,\phi)=(0.1\pi,\pi)$ and $(0.9\pi,0)$ in Figs. 5 and 6 are the combined results of the layered structure in the sheared granular material and the shear motion. Particles of neighboring layers are located in directions about $\theta=0.1\pi$ and 0.9π. The local maxima in Fig. 4 are in the downwind directions, where the shear motion carries contacting particles away and contacts are loose. The contacts in these directions are likely to be short-term contacts and result in the local maxima in Fig. 4 for short-term contacts. The local maxima in Figs. 5 and 6 are in the upwind directions in the shear flow, where particle contacts are squeezed. In these directions, contacts are likely to be long-terms ones and form the local maxima in Figs. 5 and 6 for long-terms contacts. The similarity between Figs. 5 and 6 suggests that the probability distribution $P_d(\theta,\phi|\mathbf{x},a,t)$ becomes less dependent on the age as the age increases.

For a steady system one can obtain from the probability distribution P_g of ages the probability distribution P_L of life spans. That is the probability distribution of contact age at which the contact breaks. Let N_c be the probable number of contacts in the system. For a steady system both N_c and P_g are independent of time. The probable number of contacts with ages between a and $a+\delta a$ is $N_c P_g(a)\delta a$. As time advances from t to $t+\Delta t$, $(\Delta t>0)$, the probable number of contacts with age between $a+\Delta t$ and $a+\delta a+\Delta t$ is $N_c P_g(a+\Delta t)\delta a$. The probable number difference $N_c[P_g(a)-P_g(a+\Delta t)]\delta a$ between the age groups is the number of contacts that break during that time period $[t,t+\Delta t]$. The total number of contacts that exist at time t and break during the same time period Δt, regardless of age, is $N_c\int_0^\infty[P_g(a)-P_g(a+\Delta t)]da=N_c\int_0^{\Delta t}P_g(a)da$. According to the definition of the probability distribution of contact life spans, we have

$$P_L(a)\delta a=\frac{N_c[P_g(a)-P_g(a+\Delta t)]\delta a}{N_c\int_0^{\Delta t}P_g(a)da}. \tag{10}$$

As Δt approaches zero, P_L becomes

$$P_L(a)=-\frac{1}{P_g(0)}\frac{dP_g(a)}{da}. \tag{11}$$

Since the probability distribution P_L is always non-negative, the probability distribution P_g is a nonincreasing function of age. Because the age distribution is exponential for contact ages long compared to the binary collision time in a steady simple shear flow [9], according to Eq. (11) the probability of a contact life span is also an exponential distribution for long contacts in a steady simple shear flow.

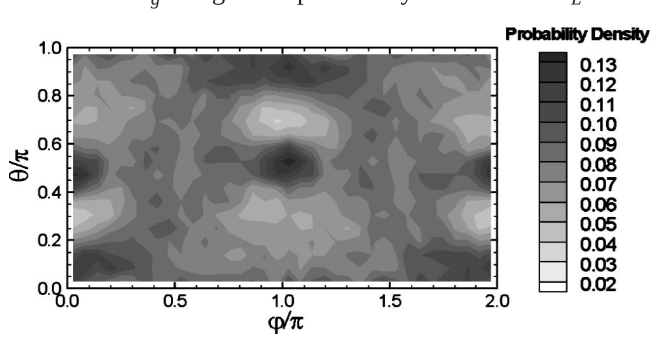

FIG. 4. Probability density of particle contacts on the particle surface for contact ages less than 0.01 time unit.

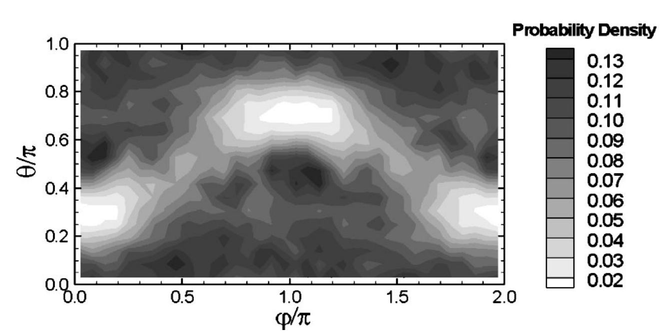

FIG. 6. Probability density of particle contacts on the particle surface for contact ages larger than 4 time units.

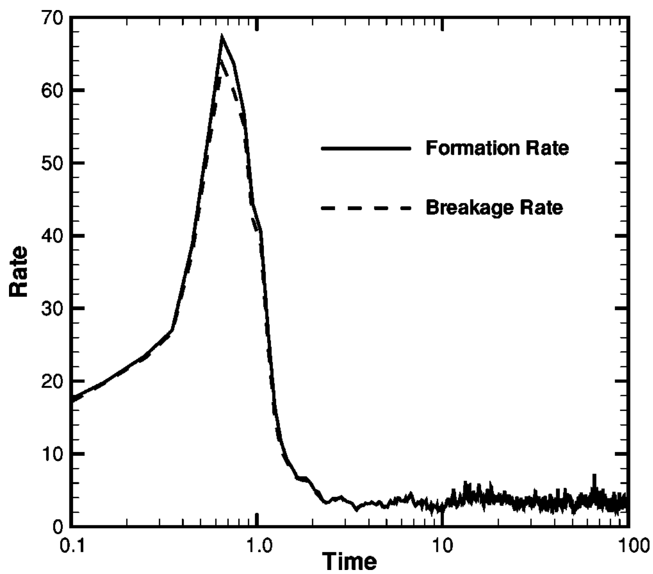

FIG. 7. Rates of particle contact formation and breakage per particle.

In a statistically steady simple shear flow, the contact generation rate and breakage rate reach a dynamical equilibrium. In Fig. 7 we show the time history of reaching the dynamical equilibrium. At the beginning of the numerical simulation, particles are not in contact. Simple shear flow is imposed on the system at time $t=0$. The nondimensional shear rate is 0.1. The contact formation rate per particle is plotted as the solid line and the contact breakage rate per particle is plotted as the dashed line in the figure. As shown in the figure, large numbers of contacts form and break shortly after the beginning of the shear and the system is very dynamic during this time period. As the system reaches the statistically steady state the system becomes less dynamic and both contact formation and breakage rates reduce. An interesting observation from this figure is that the contact formation rate and breakage rate follow each other closely. After a steady state is reached, not only the mean values of the rates are the same, but their fluctuations also follow each other closely. This is a result of the difference between the binary collision time scale and the macroscopic time scale of the dense granular flow. In a dense granular system it takes little time for a particle to form another contact after it breaks from a previous contact. For a time scale large compared to the binary collision time and the mean free flight time, the observed contact generation rate is almost the same as the contact breakage rate.

IV. STRESS RELAXATION AND THE PROBABILITY OF PARTICLE CONTACT AGES

As mentioned in the Introduction, in a dense granular flow the major granular stress is the contact stress. Following [8,9,12] the contact stress σ can be calculated as

$$\theta_p\boldsymbol{\sigma}(\mathbf{x},t)=\frac{1}{2}\int\overline{\mathbf{f}_a\mathbf{r}}(\mathbf{x},\theta,\phi,a,t)P_s(\mathbf{x},\theta,\phi,a,t)d\omega da,\tag{12}$$

where $\overline{\mathbf{f}_a\mathbf{r}}$ is the averaged tensor product of the interaction force $\mathbf{f}_a$ and the distance vector $\mathbf{r}$ between the pair of contacting particles. The overbar again denotes that the average is conditional on the specified position $\mathbf{x}$, the contact direction (θ,ϕ), and the age a at time t.

Multiplying (4) by $\overline{\mathbf{f}_a\mathbf{r}}$ leads to the equation

$$\frac{\partial(\overline{\mathbf{f}_a\mathbf{r}}P_s)}{\partial t}+\frac{\partial(\overline{\mathbf{f}_a\mathbf{r}}P_s)}{\partial a}+\nabla\cdot(\overline{\mathbf{w}}\overline{\mathbf{f}_a\mathbf{r}}P_s)+\frac{1}{\sin\theta}\frac{\partial(\overline{\dot{\theta}}\sin\theta\overline{\mathbf{f}_a\mathbf{r}}P_s)}{\partial\theta}+\frac{\partial(\overline{\dot{\phi}}\overline{\mathbf{f}_a\mathbf{r}}P_s)}{\partial\phi}=\frac{d(\overline{\mathbf{f}_a\mathbf{r}})}{dt}P_s-\frac{\overline{\mathbf{f}_a\mathbf{r}}P_s}{\tau(\mathbf{x},\theta,\phi,a,t)},\tag{13}$$

where

$$\frac{d\overline{\mathbf{f}_a\mathbf{r}}}{dt}=\frac{\partial\overline{\mathbf{f}_a\mathbf{r}}}{\partial t}+\frac{\partial\overline{\mathbf{f}_a\mathbf{r}}}{\partial a}+\overline{\dot{\theta}}\frac{\partial\overline{\mathbf{f}_a\mathbf{r}}}{\partial\theta}+\overline{\dot{\phi}}\frac{\partial\overline{\mathbf{f}_a\mathbf{r}}}{\partial\phi}+\overline{\mathbf{w}}\cdot\nabla(\overline{\mathbf{f}_a\mathbf{r}}).\tag{14}$$

Equation (12) states that the total stress is the sum of the stress components $\frac{1}{2}\overline{\mathbf{f}_a\mathbf{r}}P_sd\omega da$ contributed by contacts at different directions with difference ages. Multiplying Eq. (13) by $\frac{1}{2}d\omega da$, we find an evolution equation for these stress components. Each of these stress components has its relaxation time $\tau(\mathbf{x},\theta,\phi,a,t)$ as in the last term of Eq. (13). This is similar to the Prony series for a viscoelastic material [12]. Instead of having discrete stress components, here we have a continuous spectrum of stress components with a continuous spectrum of relaxation times.

Integration over all possible directions and all possible contact ages leads to the evolution equation for the total stress:

$$\begin{aligned}\frac{\partial(\theta_p\boldsymbol{\sigma})}{\partial t}+\nabla\cdot(\theta_p\tilde{\mathbf{w}}\boldsymbol{\sigma})=\frac{1}{2}\int\frac{d\overline{\mathbf{f}_a\mathbf{r}}}{dt}P_sd\omega da\\-\frac{1}{2}\int\frac{\overline{\mathbf{f}_a\mathbf{r}}P_s}{\tau(\mathbf{x},\theta,\phi,a,t)}d\omega da\\-\frac{1}{2}\nabla\cdot\int(\overline{\mathbf{w}}-\tilde{\mathbf{w}})\overline{\mathbf{f}_a\mathbf{r}}P_sd\omega da\\+\frac{1}{2}\int[\overline{\mathbf{f}_a\mathbf{r}}P_s]_{a=0}^{a=\infty}d\omega,\end{aligned}\tag{15}$$

where $\tilde{\mathbf{w}}$ is the unconditionally averaged velocity. The last term in Eq. (15) is, in principle, zero, because at the beginning ($a=0$) of a contact the interaction force $\mathbf{f}_a$ is zero and at $a=\infty$ the probability P_s vanishes. However, in many numerical simulations, a dashpot is used in the model for particle interaction forces. In those simulations this term is not strictly zero, but can be neglected in most of the simulations. The velocity $\overline{\mathbf{w}}$ is the averaged velocity conditional on the pair of the contacting particles. The velocity difference $\overline{\mathbf{w}}-\tilde{\mathbf{w}}$ is of the same order as the relative velocity $\mathbf{v}_r$ between the contacting pair. The displacement $(\overline{\mathbf{w}}-\tilde{\mathbf{w}})\tau$ resulting from the velocity fluctuation is of the order of the particle size—that is, much smaller than the macroscopic length scale L associated with the divergence in the third term on the right-hand side. Therefore, the third term in the right-hand side of Eq. (15) can be neglected.

Using the continuity equation [8]

$$\frac{\partial \theta_p}{\partial t} + \nabla \cdot (\theta_p \tilde{\mathbf{w}}) = 0, \tag{16}$$

we can rewrite Eq. (15) as

$$\theta_p \frac{d\boldsymbol{\sigma}}{dt} = \frac{1}{2}\int \frac{d\overline{\mathbf{f}_a\mathbf{r}}}{dt} P_s d\omega da - \frac{1}{2}\int \frac{\overline{\mathbf{f}_a\mathbf{r}} P_s}{\tau(\mathbf{x},\theta,\phi,a,t)} d\omega da, \tag{17}$$

where

$$\frac{d\boldsymbol{\sigma}}{dt} = \frac{\partial \boldsymbol{\sigma}}{\partial t} + \tilde{\mathbf{w}} \cdot \nabla \boldsymbol{\sigma} \tag{18}$$

is the material derivative of the stress. Equation (17) shows that $\boldsymbol{\sigma}$, rather than $\theta_p\boldsymbol{\sigma}$, is associated with the material point of the granular material.

For a pair with finite contact time, the value of $\overline{\mathbf{f}_a\mathbf{r}}$ can change because of the rigid-body rotation of the pair even if the deformation of the pair is held constant. The effect of rigid-body rotation is a result of kinematics of the motion. In the development of the closure models for the right-hand side of Eq. (17), it is usually more convenient to focus on the dynamics of particle interactions. To separate the kinematic effects from the dynamic effects one can introduce the corotational invariant (Jaumann) time derivative [8,9,13].

$$\frac{J\overline{\mathbf{f}_a\mathbf{r}}}{Jt} = \frac{d\overline{\mathbf{f}_a\mathbf{r}}}{dt} - \boldsymbol{\Omega} \cdot \overline{\mathbf{f}_a\mathbf{r}} + \overline{\mathbf{f}_a\mathbf{r}} \cdot \boldsymbol{\Omega}, \tag{19}$$

where $\boldsymbol{\Omega}$ is the spin tensor:

$$\boldsymbol{\Omega} = \frac{1}{2}[\nabla \tilde{\mathbf{w}} - (\nabla \tilde{\mathbf{w}})^T]. \tag{20}$$

The evolution equation (17) for the stress can be written as

$$\theta_p \frac{J\boldsymbol{\sigma}}{Jt} = \frac{1}{2}\int \frac{J\overline{\mathbf{f}_a\mathbf{r}}}{Jt} P_s d\omega da - \frac{1}{2}\int \frac{\overline{\mathbf{f}_a\mathbf{r}} P_s}{\tau(\mathbf{x},\theta,\phi,a,t)} d\omega da, \tag{21}$$

where

$$\frac{J\boldsymbol{\sigma}}{Jt} = \frac{\partial \boldsymbol{\sigma}}{\partial t} + \tilde{\mathbf{w}} \cdot \nabla \boldsymbol{\sigma} - \boldsymbol{\Omega} \cdot \boldsymbol{\sigma} + \boldsymbol{\sigma} \cdot \boldsymbol{\Omega}. \tag{22}$$

In this form the Jaumann derivative $J\overline{\mathbf{f}_a\mathbf{r}}/Jt$ is independent of rigid-body rotation. Depending on the nature of interaction forces between particles appropriated closures can be derived to close the equation [8,9].

The appearance of the Jaumann derivative is a result of changes in the directions of the particle interaction force $\mathbf{f}_a$ and the relative distance $\mathbf{r}$ during the particle contact [8]. If particle interactions are instantaneous, as assumed in kinetic theories, the particles spend no time together and the rotations in the directions of the force and the distance vector are unimportant. Therefore rotation terms do not appear in a kinetic theory for granular flows.

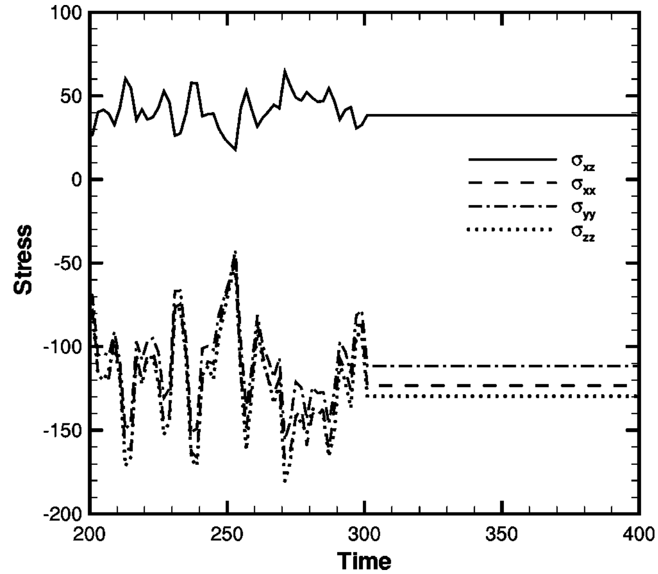

FIG. 8. Stress variation before and after a simple shear is halted. Before the nondimensional time 300, the granular material is undergoing a simple shear flow with nondimensional shear rate 0.1. The stress fluctuates during the shear motion. The shear rate is brought to zero at time 300. The stress introduced by the motion before the stopping time stays nearly unchanged afterward.

The relaxation time $\tau(\mathbf{x},\theta,\phi,a,t)$ in Eq. (17) for the stress is the same relaxation time for the probability of the contact age. Therefore the evolution of the contact age probability is closely related to the stress evolution in a dense granular material.

For long contact ages, the relaxation time is independent of the age a and orientation (θ,ϕ) [9]. Furthermore, for long contact ages the relaxation time for the age probability is inversely proportional to the shear rate γ [9],

$$\tau\gamma = c_s(\theta_p), \tag{23}$$

in a dense and slow simple shear flow, in which particle inertia is not important. According to this relation, the relaxation time for long-term contacts increases as the shear rate decreases. The rate that long-term contacts break also decreases. Therefore, as the shear rate decreases, the portion of long-term contacts increases and the fraction of contacts with contact age comparable to the binary collision time decreases. Eventually the contact stress is dominated by long-term contacts. This analysis is supported by the results of a numerical experiment, shown in Figs. 8 and 9. In the numerical simulation, the particle volume fraction is 0.6. The system is sheared with nondimensional shear rate 0.1 for 300 time units and then the shear rate is suddenly reduced to zero. According to Eq. (23) the stress relaxation time becomes infinity and the breakage rate for long age contacts is zero after the cessation of the shear. Therefore the stress resulting from long-age contacts does not relax. The shear stress and three normal stresses are plotted as functions of time in Fig. 8. Little stress reduction is observed in Fig. 8. Figure 9 provides a close-up look at the stress variations around the time when the shear motion is abruptly stopped.

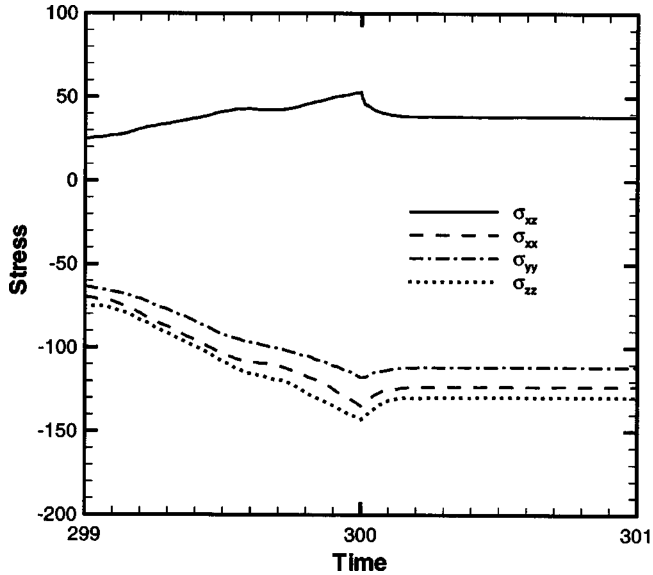

FIG. 9. A close-up look of the stress variation around the stopping time. Only a short period of stress relaxation is observed.

After stopping the externally driven shear motion the stress drops in a short amount of time (about 0.2 time units) and then reaches a steady state. During this short time period, loose particle contacts, including those involving binary collisions, break. Breaking of these contacts causes about a 20% reduction in the shear stress and a less than 10% reduction in the normal stresses, while the typical stress fluctuation in this case is more than 30% as shown in Fig. 8. A long stress relaxation time is observed in experiments of a Couette flow [14] after the shear motion is stopped.

Although the time scale of the stress relaxation in the experiment [14] is much larger than the time scales in the numerical simulation described above, the stress relaxation in the experiment is also related to the relaxation of contact probability. For a sheared granular system, the slow stress decay observed in the experiments is related to slow rearrangements of particle contacts and settling of the granular material. After stopping the shear the major force in the system is carried by force chains. It seems reasonable to speculate that the sheared granular material is under constant small perturbations from the environment. For a contact, the longer it has existed, the less likely it is to break because, when it has withstood perturbations in the past, it is more likely to withstand similar perturbations in the future. Therefore it is reasonable to assume that during the slow relaxation the relaxation rate is

$$\frac{1}{\tau}=\frac{c_p}{a}=\frac{c_p}{t-t_0}, \tag{24}$$

where c_p is a constant related to the probability relaxation and t_0 is the time when the contact is formed. Furthermore, the contact age a is the only relevant time scale in this case. Breaking a contact can result in rearrangement of particles in force chains around the contact and results in a force change; therefore, the time scale for the force change is the same as the probability relaxation and the Jaumann derivative (19) of $\mathbf{f}_a\mathbf{r}$ can be written as

$$\frac{J\overline{\mathbf{f}_a\mathbf{r}}}{Jt}=\frac{d\overline{\mathbf{f}_a\mathbf{r}}}{dt}=\frac{c_f\overline{\mathbf{f}_a\mathbf{r}}}{a}=\frac{c_f\overline{\mathbf{f}_a\mathbf{r}}}{t-t_0}. \tag{25}$$

By substituting Eqs. (24) and (25) into the stress evolution equation (21), we have

$$\theta_p\frac{d\boldsymbol{\sigma}}{dt}=-\frac{c_\ell}{2(t-t_s)}\int d\omega\int_0^{t_s}\overline{\mathbf{f}_a\mathbf{r}}P_s\frac{t-t_s}{t-t_0}dt_0, \tag{26}$$

where $c_\ell=c_p-c_f$ and t_s is the time when the shear stopped. In writing this equation we have neglected the contributions from the contacts formed after shearing is stopped because the interaction forces in these contacts are small compared to those of the contacts formed during the shear. During the slow stress relaxation $t\gg t_s$, the factor $(t-t_s)/(t-t_0)\approx 1$ and the equation becomes

$$\frac{d\boldsymbol{\sigma}}{dt}=-\frac{c_\ell\boldsymbol{\sigma}}{t-t_s} \tag{27}$$

after the use of Eq. (12). The solution of this equation is

$$\boldsymbol{\sigma}=\left(\frac{t_b-t_s}{t-t_s}\right)^{c_\ell}\boldsymbol{\sigma}^b, \tag{28}$$

where $\boldsymbol{\sigma}^b$ and t_b are the stress and time at the beginning of the slow stress relaxation.

The assumptions (24) and (25) lead to a power-law decay of the stress. This seems to contradict the logarithmic stress decay observed in the experiment [14]. However, in experiment the stress changes less than 2% during the slow relaxation. By writing Eq. (28) in component form and taking the logarithm of both sides, we have

$$\ln\left(1+\frac{\sigma_{ij}-\sigma_{ij}^b}{\sigma_{ij}^b}\right)=-c_\ell\ln\left(\frac{t-t_s}{t_b-t_s}\right). \tag{29}$$

The left-hand side of this equation can be expanded by a Taylor's series. Upon keeping the first term in the series for small $(\sigma_{ij}-\sigma_{ij}^b)/\sigma_{ij}^b$, we have

$$\boldsymbol{\sigma}\approx\left[1-c_\ell\ln\left(\frac{t-t_s}{t_b-t_s}\right)\right]\boldsymbol{\sigma}^b. \tag{30}$$

This analysis implies that for small stress changes during the slow relaxation, it is difficult to distinguish a power-law decay from a logarithmic decay. To distinguish these two decay laws, higher-order terms in the stress, such as $[(\sigma_{ij}-\sigma_{ij}^b)/\sigma_{ij}^b]^2$, need to be measured accurately. If there is a time scale during which the logarithmic stress decay law is obeyed, then there must exist another larger time scale at which the stress ceases to obey the logarithmic law. Otherwise, as time increases, the stress will eventually change sign, which of course cannot happen in a granular material without a macroscopic motion. If the stress obeys a power-law decay, no additional time scale is necessary. Clearly, to resolve these issues, experiments with a much longer observation time are necessary, and the assumptions (24) and (25) leading to the power-law stress decay need to be checked

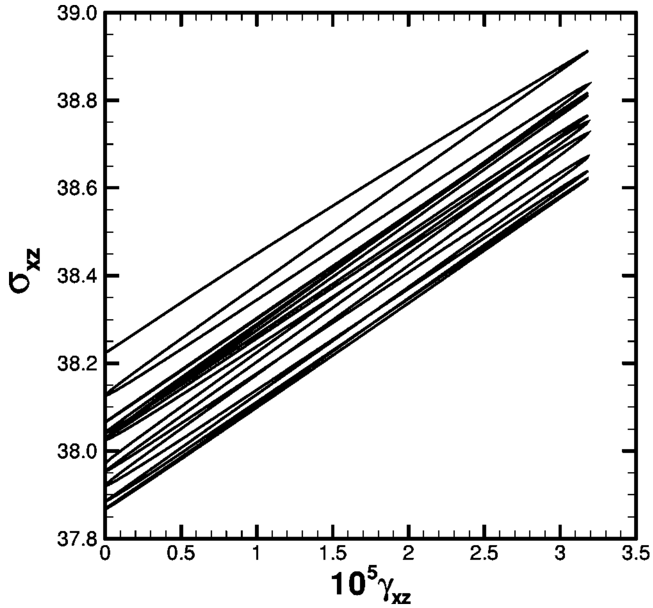

FIG. 10. After subjecting a granular material to steady shear, an oscillatory shear is imposed on the material. For a short period (10^{-3} time unit) or high frequency of the oscillatory motion, the stress-strain relation is linear for each shearing cycle while the stress relaxes at a larger time scale than the period of the shear motion.

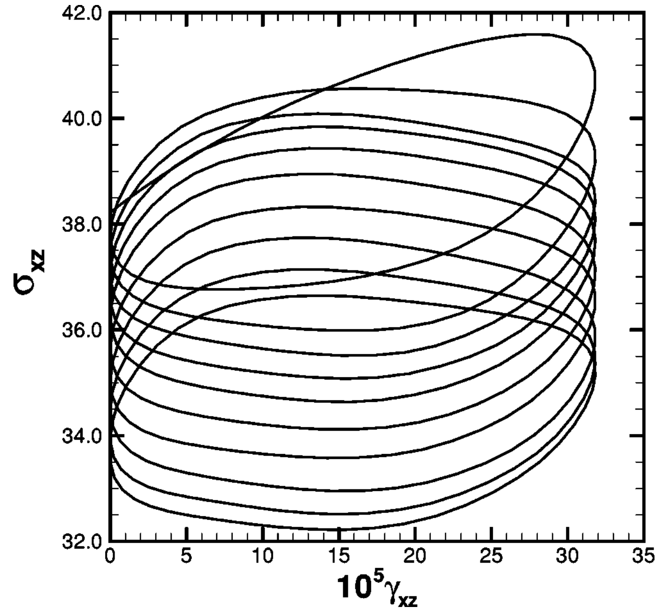

FIG. 11. For a longer period (10^{-2} time unit) or lower frequency of the oscillatory motion, the stress-strain relation forms not only loops but also is not monotonic during a shearing cycle while the stress relaxes at a larger time scale than the period of the shear motion.

carefully against the experiments. For a compressed system in which particles are squeezed tightly together, small perturbations from the environment are less likely to cause breakage of contacts and the stress does not relax [14].

Since the stress relaxation is closely related to the age probability distribution function and Fig. 1 shows a spectrum of the age probability relaxation times, we expect to see different stress relaxation behaviors when different frequencies of oscillatory shear are imposed on the granular system. For this purpose, we simulate a granular medium undergoing oscillatory shear motion. An oscillatory shear motion is imposed on the granular material after it is sheared by the steady shear motion for 300 time units as described above. According to Fig. 1, the probability of the contact age does not relax and $1/\tau(\mathbf{x},\theta,\phi,a,t)\approx 0$ for contacts with age smaller than the binary collision time. For an oscillatory shear with a period less than the binary collision time, the stress relaxation can be neglected and the material behaves elastically during a shear cycle. Also according to Fig. 1, a significant relaxation of the age probability distribution happens when the age is close to the binary collision time 5.0×10^{-3} for the linear spring and dashpot force model used in the simulation. We therefore predict that significant stress relaxation is observable in that time scale. This is indeed true, as shown in Fig. 10 where the shear stress is plotted as a function of shear deformation. The amplitude of the sinusoidal shear rate is 0.1 and the period is 10^{-3}. Figure 10 shows that there is no phase delay and the stress-strain relation is almost linear for each of the ten cycles that are plotted. The decrease in the peak stress is mainly due to the stress relaxation at the binary collision time scale as predicted.

For a sinusoidal shear with a period larger than the binary collision time we expect a significant phase delay in the stress-strain relation. To demonstrate this, we simulate an oscillatory shear of the same amplitude but with period 10^{-2} time unit. The resulting stress-strain relation is plotted in Fig. 11. The stress-strain relation not only forms loops but also has a phase delay as the stress and strain reach their peaks at different times. The decay of the peak stresses in Fig. 11 is a result of a relaxation time longer than the period of the oscillatory shear in the spectrum of the relaxation times indicated in Fig. 1.

The numerical simulations mentioned in this paper are performed using nondimensional numbers. To provide a connection between these numerical simulations and real experiments, let us now suppose the particles are sand grains about 100 μm in size. It is estimated [9] that the binary collision time of the grains is of order 10 μs. As mentioned in Sec. III, a time unit in this simulation is 100 periods of the mass-spring system or about 2 ms for the sand. The non dimensional shear rate 0.1 simulated above corresponds to shear rate 50 s^{-1} for the sand.

V. CONCLUSIONS

The evolution of the probability distribution of particle contact ages is found to be important to the evolution of the stresses in a dense granular system. The age of a particle contact is defined as the difference between the current time and the time when the contact was formed. The relaxation rate of the probability distribution is the contact breakage rate and is directly related to stress relaxation in the system. In a dense and slow granular flow in which particle inertia can be neglected, particle contact formation rate is small and most contacts have ages that are long compared to the binary collision time. Interaction forces in long-age contacts are larger than that in short-age contacts. Therefore the stress in a dense and slow granular flow is mostly due to long-age contacts.

For a dense and slow granular flow, numerical simulations show that the relaxation time of the probability distribution of long contact ages is inversely proportional to the macroscopic strain rate. There is a spectrum of time scales for the relaxation of the contact-age probability distribution. The smallest time scale is the binary collision time. This spectrum of relaxation rates results in different stress relaxation time scales that lead to different behaviors of the phase delay in the stress-strain relations under dynamic loadings. While the constitutive relation for the granular material can be written in a form [9] similar to many viscoelastic materials such as polymers, the stress relaxation as a result of contact breaking behaves differently from a typical polymer. A typical polymer behaves like solid if the macroscopic time scale is small compared to the stress relaxation time of the material and like a fluid if the macroscopic time scale is large. Similar to a typical polymer, a dense granular material behaves like a solid when the macroscopic time scale is small compared to the binary collision time because particle contacts have no time to break. For a finite strain rate, the dense granular material has a finite relaxation time and behaves as a viscoelastic fluid. A flow of granular material causes dilation that reduces the particle volume fraction and the relaxation time if the material is not well confined. When the relaxation time is reduced, the material behaves more like fluid. However, for the slow simple shear flow simulated in this paper, where the material is well confined in the directions perpendicular to the flow, the dense granular material behaves like a solid as the strain rate approaches zero. This is because the relaxation time in the dense granular material increases as the strain rate decreases, while the relaxation time for a typical polymer is independent of or a weak function of the macroscopic strain rate.

ACKNOWLEDGMENTS

The author would like to acknowledge many important discussions with Dr. F. H. Harlow, Professor J. T. Jenkins at Cornell University, Dr. R. M. Rauenzahn, Professor H. Shen at Clarkson University, and Dr. X. Ma. The Joint DOD/DOE Munitions Technology Development Program provided the financial support for this work.

[1] J. T. Jenkins and S. B. Savage, J. Fluid Mech. **130**, 187 (1983).
[2] C. K. K. Lun, S. B. Savage, D. J. Jeffrey, and N. Chepurniy, J. Fluid Mech. **140**, 223 (1984).
[3] J. T. Jenkins and M. W. Richman, Phys. Fluids **28**, 3485 (1985).
[4] J. T. Jenkins and Cao Zhang, Phys. Fluids **14**, 1228 (2002).
[5] C. Campbell, J. Fluid Mech. **465**, 261 (2002).
[6] H. Hwang and K. Hutter, Continuum Mech. Thermodyn. **7**, 357 (1995).
[7] M. Louge, Phys. Rev. E **67**, 061303 (2003).
[8] D. Z. Zhang and R. M. Rauenzahn, J. Rheol. **41**, 1275 (1997).
[9] D. Z. Zhang and R. M. Rauenzahn, J. Rheol. **44**, 1019 (2000).
[10] C. Cercignani, *The Boltzmann Equation and its Applications* (Springer-Verlag, New York, 1988).
[11] M. Alam and S. Luding, Phys. Fluids **15**, 2298 (2003).
[12] D. Z. Zhang, C. Liu, and F. H. Harlow, Phys. Rev. E **66**, 051806 (2002).
[13] D. D. Joseph, *Fluid Dynamics of Viscoelastic Liquids* (Springer-Verlag, New York, 1990).
[14] R. R. Hartley and R. P. Behringer, Nature (London) **421**, 928 (2003).